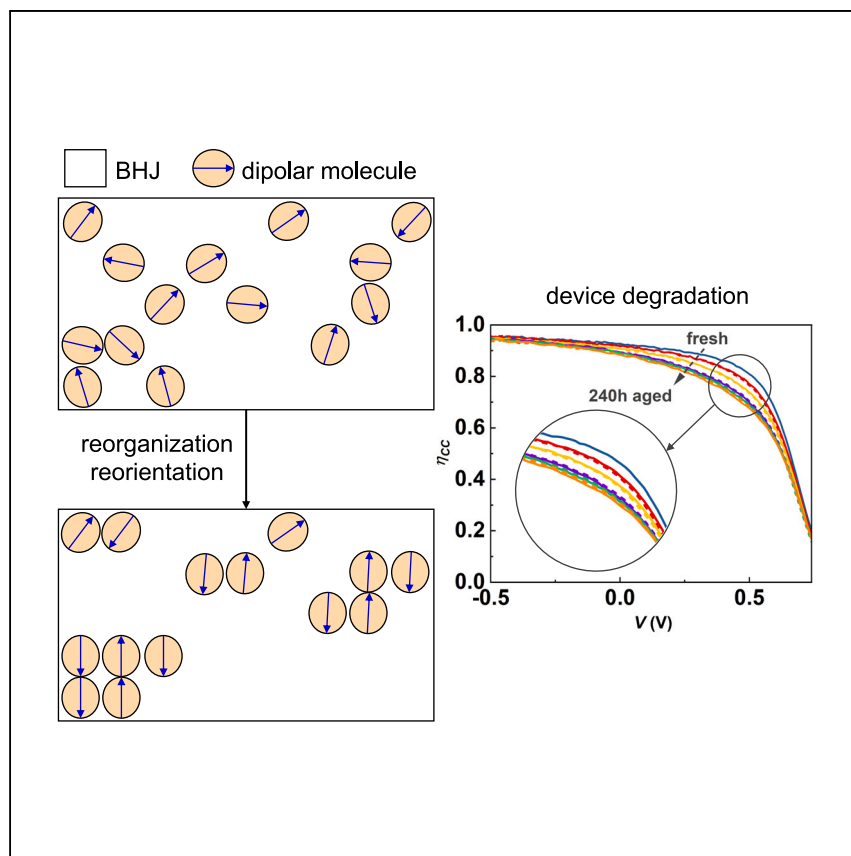


Article

Impact of dipolar molecules on the reliability of organic photovoltaic cells



The dipolar molecules in organic photovoltaic devices are shown by Huang et al. to aggregate and align anti-parallel to neighboring molecules during device operation. The dipolar reorganization results in an increased dielectric constant within the photoactive region, leading to reduced photocurrent extraction and device performance over time.

Xinjing Huang, Yongxi Li,
Stephen R. Forrest

stevefor@umich.edu

Highlights

Dipolar molecules result in reduced device reliability of organic photovoltaics

Dipolar molecules tend to reorganize and reorient during device operation

Dipolar reorganization leads to increased dielectric constant and reduced performance

Article

Impact of dipolar molecules on the reliability of organic photovoltaic cells

Xinjing Huang,¹ Yongxi Li,² and Stephen R. Forrest^{1,2,3,4,*}

SUMMARY

Blending two non-fullerene acceptors (NFAs) to form bulk heterojunctions (BHJs) in ternary organic photovoltaics (OPVs) has been shown to lead to an end-capping exchange reaction that results in the generation of several new dipolar species whose impact on OPV operational stability remains uncertain. Here, we investigate the reliability of a ternary OPV system intentionally blended with dipolar NFA molecules. We reveal that an intrinsic contribution to OPV degradation is the reorganization and reorientation of the dipolar molecules during operation, which leads to an increased dielectric constant (ϵ_r) of the BHJ. Consequently, the electric field across the BHJ with dipolar molecules decreases compared with that of a non-dipolar BHJ under the same applied voltage, leading to a larger reduction in charge collection efficiency over time. This result has implications on the stability of a range of organic electronic devices containing dipolar molecules.

INTRODUCTION

Organic photovoltaics (OPVs) are emerging as an attractive solution to solar energy harvesting due to their distinct advantages of light weight, semitransparency, flexibility, and environmental compatibility.¹ By introducing dipolar molecules in OPV bulk heterojunctions (BHJs), the power conversion efficiency (PCE) can be improved due to the change of intramolecular electron-hole separation as well as a modified molecular packing.^{2–5} The past few decades have witnessed substantial developments in employing dipolar materials in OPVs such as donor-acceptor-acceptor' (d-a-a')-type small-molecule donors^{3,6–10} and asymmetric non-fullerene acceptors (NFAs).^{2,5,11–15} Recently, however, it has been shown that end-capping reactions between two acceptor-donor-acceptor (a-d-a)-type NFAs in ternary OPVs can generate dipolar reaction products that reduce the device operational stability.¹⁶

In this work, we explore the impact of dipolar molecules on device reliability by studying a ternary OPV system intentionally blended with dipolar molecules that are among the products of end-capping exchange reactions. We find that the devices with a higher ratio of dipolar constituents show a larger decrease in charge collection efficiency (η_{CC}) and PCE after aging compared with devices with fewer or no dipolar components. Here, η_{CC} is the ratio between the photocurrent, J_{ph} (V), at voltage, V , and the saturated photocurrent, $J_{ph,sat}$, at large reverse bias. We attribute these changes to an increase in the relative dielectric constant (ϵ_r) in the dipolar BHJ, which in turn leads to a decrease in the internal electric field. Measurements suggest that the ϵ_r of the BHJ (ϵ_{BHJ}) containing only non-polar molecules

¹Applied Physics Program, University of Michigan, Ann Arbor, MI 48109, USA

²Department of Electrical Engineering and Computer Science, University of Michigan, Ann Arbor, MI 48109, USA

³Department of Physics, Department of Material Science and Engineering, University of Michigan, Ann Arbor, MI 48109, USA

⁴Lead contact

*Correspondence: stevefor@umich.edu
<https://doi.org/10.1016/j.xcrp.2023.101551>



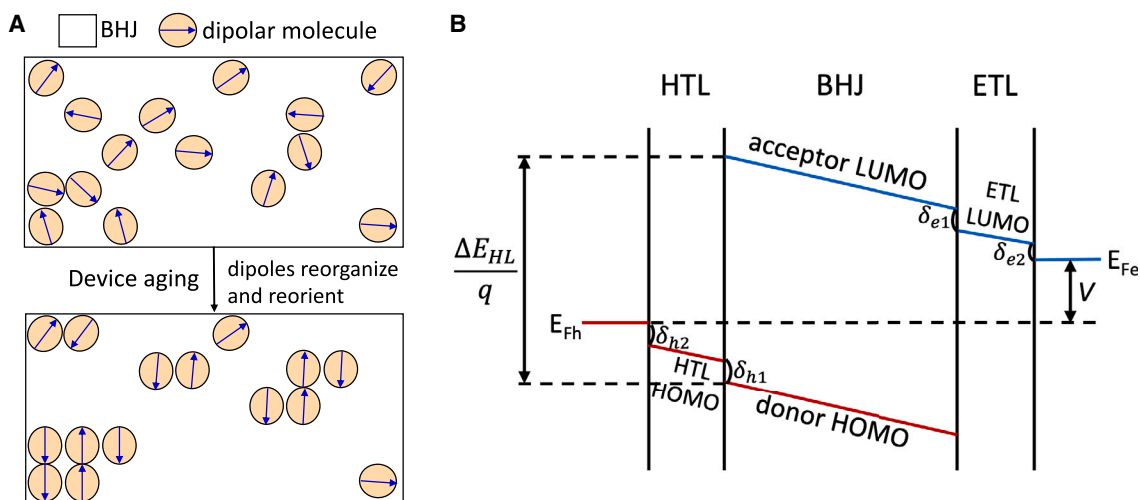


Figure 1. Dipolar molecule reorganization and electric field distribution in organic photovoltaics (OPVs)

(A) Illustration of dipolar molecule reorganization in the bulk heterojunction (BHJ) of OPV during device operation to reach lower energy configurations. (B) Energy-level diagram of an OPV at applied voltage V , including voltage drops (δ) across the BHJ, the charge transporting layers, and various interfaces.

remains stable after 240 h aging under white light illumination at 10 sun intensity, while it significantly increases under the same conditions when the medium contains dipolar molecules. To understand the origin of the change in ϵ_r , we perform Monte Carlo simulations of dipole orientations that indicate that the dipolar molecules tend to aggregate and align anti-parallel to neighboring molecules, which accurately predicts the change in η_{CC} , and hence the PCE, during extended periods of device operation.

RESULTS AND DISCUSSION

Dipole reorganization and electric field distribution

When the devices undergo aging, dipolar molecules in the BHJ can reorganize and reorient to reach lower energy configurations¹⁷ (see Figure 1A). The energy due to dipole-dipole interactions is calculated using the dipole interaction energy:

$$E = \sum \frac{1}{4\pi\epsilon_r\epsilon_0 r_{ij}^3} [\vec{p}_i \cdot \vec{p}_j - 3(\vec{p}_i \cdot \hat{r}_{ij})(\vec{p}_j \cdot \hat{r}_{ij})], \quad (\text{Equation 1})$$

where ϵ_r is the relative dielectric constant of the medium, ϵ_0 is the vacuum permittivity, r_{ij} is the distance between the i^{th} and j^{th} molecules, \hat{r}_{ij} is the unit vector between them, and \vec{p}_i and \vec{p}_j are their dipole moments. The total dipole moment is the sum of permanent, \vec{p}_0 , and induced dipoles, $\vec{p} = \vec{p}_0 + \alpha \vec{F}$, with polarizability, α , and electric field, \vec{F} .

The reorganization of dipoles within a layer over time, t , results in a change in the screening of electric field. This is reflected by a change in the dielectric constant such that $(\epsilon_r(t) - \epsilon_{r,0})/(\epsilon_r(0) - \epsilon_{r,0}) = V_{int}(t)/V_{int}(0)$ (see supplemental experimental procedures for details). Here, $\epsilon_{r,0}$ is the relative dielectric constant of the non-dipolar medium, and $V_{int}(t)$ is the internal voltage due to the addition of dipoles.

As shown in Figure 1B, assuming a uniform electric field within each layer, and assuming the normal displacement field is constant across the layer interfaces, the voltage, V , across the OPV is described by

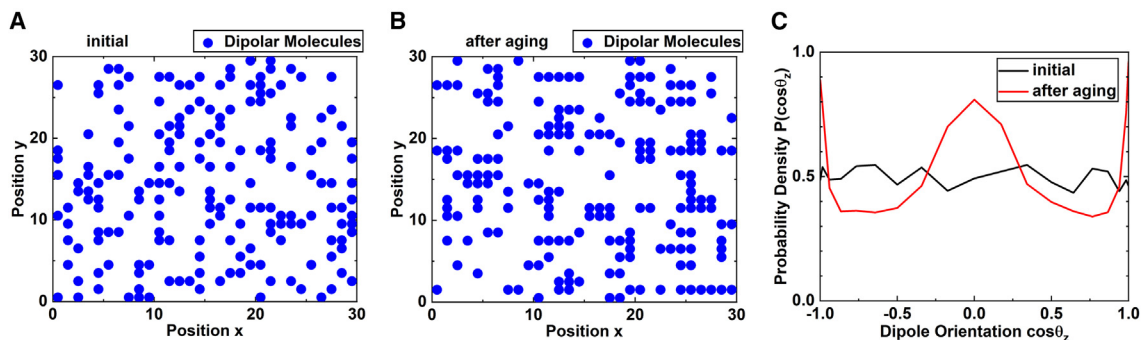


Figure 2. Simulated morphology of an acceptor blend containing dipolar molecules

(A and B) The plan view of the simulated distribution of 20% dipolar molecules in an acceptor blend (A) before and (B) after aging. (C) Simulated probability density distribution of dipole orientations before and after aging.

$$V = \frac{\Delta E_{HL}}{q} - F_{BHJ}d_{BHJ} - F_{HTL}d_{HTL} - F_{ETL}d_{ETL} - \delta_{e1} - \delta_{e2} - \delta_{h1} - \delta_{h2} \quad (\text{Equation 2})$$

and

$$\epsilon_{HTL}F_{HTL} = \epsilon_{BHJ}F_{BHJ} = \epsilon_{ETL}F_{ETL}, \quad (\text{Equation 3})$$

where ΔE_{HL} is the energy offset between the highest occupied molecular orbital (HOMO) of the donor and the lowest unoccupied MO (LUMO) of the acceptor; q is the electron charge; F_{BHJ} , F_{HTL} , and F_{ETL} are the normal electric fields across the BHJ, the hole-transporting layer (HTL), and the electron-transporting layer (ETL), respectively; d_{BHJ} , d_{HTL} , and d_{ETL} are the thicknesses of the corresponding three layers; ϵ_{BHJ} , ϵ_{HTL} , and ϵ_{ETL} are their relative dielectric constants; and δ_{e1} , δ_{e2} , δ_{h1} , and δ_{h2} are the voltages across various interfaces in Figure 1B whose dependence on V is negligible in the absence of a large density of interfacial trap states.^{18,19} When there is no electric field across the BHJ, the probability for photocurrent generation is low due to lack of a driving force to help photogenerated charges overcome Coulomb attraction and guide them toward electrodes. Therefore, we approximate that the photocurrent density $J_{ph} = 0$ when $F_{BHJ} = F_{HTL} = F_{ETL} = 0$.¹⁹ Then, Equation 2 becomes

$$V|_{J_{ph}=0} = \frac{\Delta E_{HL}}{q} - \delta_{e1} - \delta_{e2} - \delta_{h1} - \delta_{h2}, \quad (\text{Equation 4})$$

and F_{BHJ} is given by

$$F_{BHJ} = \frac{(V|_{J_{ph}=0} - V)}{\left(\frac{\epsilon_{BHJ}}{\epsilon_{HTL}}d_{HTL} + d_{BHJ} + \frac{\epsilon_{BHJ}}{\epsilon_{ETL}}d_{ETL}\right)} \quad (\text{Equation 5})$$

It is apparent from Equation 5 that an increased ϵ_{BHJ} can reduce the electric field across the BHJ, leading to a reduced η_{CC} .

A Monte Carlo-based simulated annealing (SA) protocol is used to model dipolar reorganization in the thin film.^{20–24} The simulation begins with a random distribution and orientation of dipolar molecules and then performs stepwise trial moves and rotations on the dipoles. Each step that lowers the system energy is accepted, whereas the probability for endothermic steps is weighted by a Boltzmann factor.²⁵ Figures 2A and 2B show the simulated morphology of an acceptor blend with 20% dipolar molecules before and after aging, respectively. Figure 2A is the plan view of the initial distribution of dipoles, whereas the dipoles form clusters after the

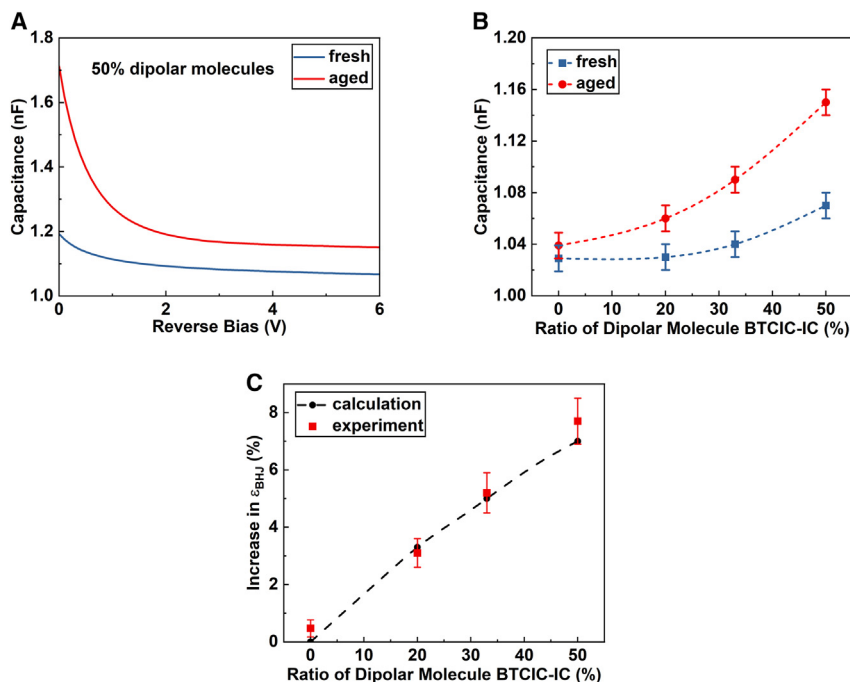


Figure 3. Capacitance-voltage (C-V) characteristics of OPV devices

(A) C-V characteristics of OPVs before and after 240 h aging under illumination at 10 sun intensity with a BHJ comprising 50% dipolar non-fullerene acceptor (NFA) molecules (BT-IC:BT-CIC:BTCIC-IC = 1:1:2).

(B) Capacitance of OPVs vs. dipolar NFA concentration before and after 240 h aging.

(C) Calculated and measured (from C-V data) increase in the relative dielectric constants (ϵ_r) of BHJs vs. BTCIC-IC ratio.

Data in (B) and (C) are represented as mean \pm standard error of the mean (SEM).

system approaches equilibrium following SA, as shown in Figure 2B. The normalized probability density distribution of the dipolar orientation, defined by the angle between the dipole moment and the substrate normal, θ_z , before and after SA is illustrated in Figure 2C. The orientation of dipoles after aging shows higher probability at $\theta_z = 0, \pm\frac{\pi}{2},$ and π due to anti-parallel dipole alignment between neighboring molecules. The change in ϵ_r is then found by calculating V_{int} induced by dipoles (see Figure S1). The NFA blend with 20% dipolar content experiences a 5.6% increase in ϵ_r . As the ϵ_r of the polymer donor (40 wt % in the BHJ) is unchanged, ϵ_{BHJ} is increased by only 3.3%. With a higher ratio of dipolar content, similar calculations result in an increase of 7% in ϵ_{BHJ} for a 50% dipolar concentration.

Change in dielectric constant over aging

To systematically investigate the impact of dipolar molecules on device stability, we fabricated ternary OPVs comprising one polymer donor, PCE-10, and two nonpolar NFAs, BT-IC and BT-CIC (see molecular and device structures in Figure S2). Their end-capping exchange product, the dipolar molecule BTCIC-IC, is blended into the NFAs with ratios of 0%, 20%, 33%, and 50%. As shown quantitatively in a previous study on the chemical reaction, such concentrations of dipolar products are in fact present in NFA-based ternary devices.¹⁶ Figure 3A shows the capacitance-voltage (C-V) characteristics of a device with 50% dipolar molecules (BT-IC:BT-CIC:BTCIC-IC = 1:1:2) before and after 240 h aging under white light illumination at 10 sun intensity (complete C-V data are in Figure S3). The dielectric constant is determined assuming the fully depleted reverse-biased diodes (at -6 V) are parallel plate capacitors. Figure 3B summarizes the

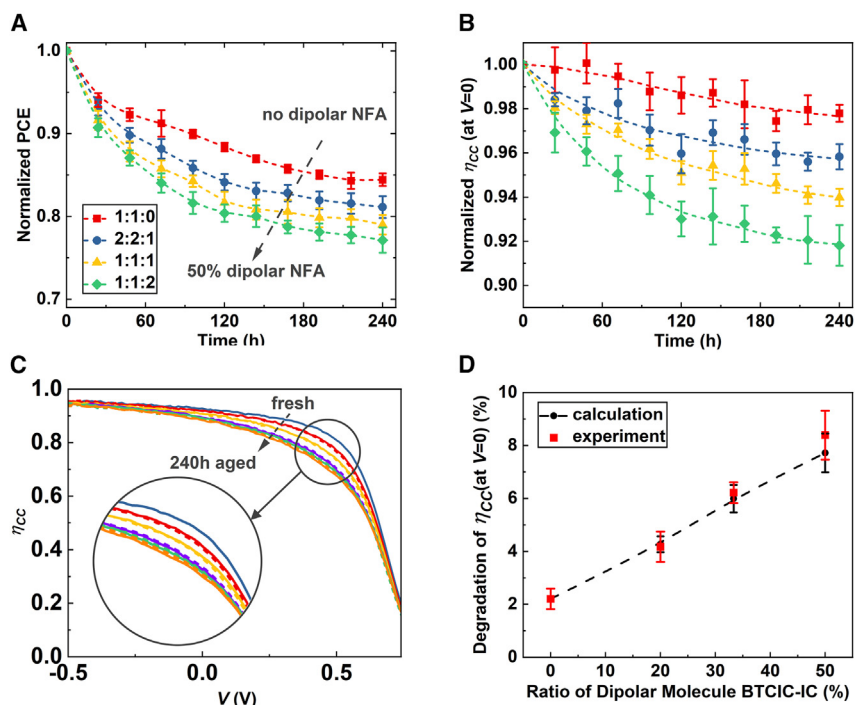


Figure 4. Evolution of OPV performance with time

(A and B) Degradation in (A) power conversion efficiency (PCE) and (B) charge collection efficiency (η_{CC} ; at $V = 0$) of OPVs with different blend ratios BT-IC:BT-CIC:BTCIC-IC over 240 h aging under illumination at 10 sun intensity. Data are represented as mean \pm SEM.

(C) Measured η_{CC} vs. V (solid lines) of OPVs comprising 20% dipolar NFA with time, along with calculated characteristics (dashed lines) of the aged device. The inset is a magnified view of the curves around the maximum power point.

(D) Measured and calculated degradation in η_{CC} (at $V = 0$) after 240 h aging of OPVs vs. ratios of dipolar BTCIC-IC. Data are represented as mean \pm SEM.

capacitance of devices containing different NFA compositions before and after aging. When there is no dipolar component in the BHJ (BT-IC:BT-CIC:BTCIC-IC = 1:1:0), C (and hence, ϵ_{BHJ}) before and after aging is unchanged at 1.03 ± 0.01 nF, while ϵ_{BHJ} increases by $7.7\% \pm 0.8\%$ for a dipolar concentration of 50%. In Figure 3C, the dashed line represents the simulated increase in ϵ_{BHJ} vs. dipolar concentration, which is consistent with that obtained from the C-V measurements, indicating that the changes in ϵ_{BHJ} can primarily be attributed to the reorganization and the reorientation of dipolar molecules over time. In addition, the carrier density calculated from C-V measurements at 0 V of the device containing 50% dipolar molecules decreases by $21\% \pm 3\%$ compared with that without dipolar content (see Figure S4), suggesting that the dipolar molecules may trap charges in the BHJ.

Evolution of device performance over aging

The evolution of device performance under 10 sun intensity illumination is shown in Figure 4A. The aging under high-intensity illumination accelerates the degradation to distinguish differences between device stabilities in a reasonable amount of time. The degradation under such a condition was found to accurately reflect the degradation under AM 1.5G illumination with an appropriate acceleration factor.^{26–28} Compared with the device lacking dipolar content where the PCE was reduced by $15.5 \pm 0.8\%$ after 240 h, the devices comprising 20%, 33%, and 50% dipolar NFAs show reductions of $18.9\% \pm 1.2\%$, $21.1\% \pm 1.1\%$ and $23.2\% \pm 1.4\%$, respectively. While the open-circuit

voltage (V_{oc}) remains relatively constant, the short-circuit current (J_{sc}) and the fill factor (FF) decrease more in devices containing dipolar molecules, as shown in Figure S4, and Figure 4B shows the decrease of η_{CC} (at $V = 0$) where devices with 20%, 33%, and 50% dipolar molecules experience $4.2\% \pm 0.5\%$, $6.2\% \pm 0.4\%$, and $8.3 \pm 0.9\%$ decreases in η_{CC} (at $V = 0$) over the aging period, whereas only a $2.2\% \pm 0.4\%$ reduction is observed in the non-polar device.

Figure 4C shows the measured as-grown and aged η_{CC} vs. V of a device with 20% BTCIC-IC, as well as the calculated reduction in η_{CC} using Equation 5 based on an increased dielectric constant over time. Here, we assume the reduction of η_{CC} is the same for all devices with and without dipolar molecules at the same F_{BHJ} . The calculated η_{CC} vs. V of OPVs with the 20% dipolar molecule concentration is shown as dashed lines, which is consistent with measurement. Figure 4D summarizes the measured and calculated changes in η_{CC} (at $V = 0$) vs. dipolar concentration. The agreement between calculation and experiment indicates that the loss in η_{CC} of devices containing dipolar molecules is primarily due to the increased ϵ_{BHJ} and the corresponding reduction in F_{BHJ} .

Recently, studies of multilayer organic light-emitting diodes (OLEDs) have also revealed polarization-induced charge accumulation at layer interfaces resulting from the presence of dipolar molecules,^{29–36} as well as the reorientation of dipoles during operation and its effect on device stability.^{37–39} Those investigations have primarily focused on the exciton-polaron quenching and charge injection at interfaces dominated by interfacial charges. In contrast, our work reveals that dipolar molecules affect the electric field distribution in the bulk of the OPVs. In both cases, our work suggests that dipolar reorganization can result in unstable performance in a range of organic electronic devices. It should be noted here that we demonstrated the impact of dipolar molecules on OPV reliability, but this is not the only mechanism contributing to reduced device performance over time. For example, the constituents arising from end-capping exchange might lead to faster degradation compared to the intentionally blended molecules discussed in this work, even though they have the same dipolar components.¹⁶ This indicates that the interactions between NFAs during solution preparation may lead to additional degradation mechanisms than those considered here. That is, the stability comparison between different materials systems should not be based solely on the concentration of dipole moments since chemical or thermal effects may also play important roles that determine device reliability.

In summary, we demonstrated that dipolar molecules in the BHJ of OPVs aggregate and align anti-parallel to neighboring molecules during device aging, resulting in increased dielectric constant, which in turn reduces the electric field across the BHJ. This change manifests itself in a decreased charge collection and hence a decreased PCE of the OPV. With a higher ratio of dipolar molecules in the BHJ, the increase in ϵ_r as well as the loss in η_{CC} and PCE are intensified. The foregoing analysis suggests that dipolar molecules in organic electronic devices can negatively impact their operational stability due to their time-dependent reorientation, which affects the electric field within the thin films of which they are comprised.

EXPERIMENTAL PROCEDURES

Resource availability

Lead contact

Further information and requests for resources and materials should be directed to and will be fulfilled by the lead contact, Stephen R. Forrest (stevefor@umich.edu).

Materials availability

This study did not generate new unique materials.

Data and code availability

The data that support this study are available from the lead contact upon reasonable request. The mathematical methods and algorithms are described in the main text and [supplemental experimental procedures](#).

SUPPLEMENTAL INFORMATION

Supplemental information can be found online at <https://doi.org/10.1016/j.xcrp.2023.101551>.

ACKNOWLEDGMENTS

This work was supported by the US Department of Energy's Office of Energy Efficiency and Renewable Energy (EERE) under Solar Energy Technologies Office (SETO) Agreement Number DE-EE0008561, and the US Office of Naval Research under Award Number N00014-17-1-2211. This report was prepared as an account of work sponsored by an agency of the United States government. Neither the United States government nor any agency thereof, nor any of its employees, makes any warranty, express or implied, or assumes any legal liability or responsibility for the accuracy, completeness, or usefulness of any information, apparatus, product, or process disclosed, or represents that its use would not infringe privately owned rights. Reference herein to any specific commercial product, process, or service by trade name, trademark, manufacturer, or otherwise does not necessarily constitute or imply its endorsement, recommendation, or favoring by the United States government or any agency thereof. The views and opinions of authors expressed herein do not necessarily state or reflect those of the United States government or any agency thereof. The authors also acknowledge Universal Display Corporation for partial funding of this work.

AUTHOR CONTRIBUTIONS

X.H. designed and conducted the calculations and experiments. Y.L. assisted with the analysis of results. S.R.F. supervised and supported the project. All authors contributed to the preparation of the manuscript.

DECLARATION OF INTERESTS

S.R.F. has an equity interest in one of the sponsors of this research (Universal Display Corp., UDC). This conflict is under management by the University of Michigan Office of the Vice President for Research. Also, U-M has a royalty-bearing license from UDC.

Received: June 14, 2023

Revised: July 19, 2023

Accepted: August 1, 2023

Published: August 21, 2023

REFERENCES

- Forrest, S.R. (2020). *Organic Electronics: Foundations to Applications* (Oxford University Press).
- Song, J., and Bo, Z. (2023). Asymmetric molecular engineering in recent nonfullerene acceptors for efficient organic solar cells. *Chin. Chem. Lett.* 34, 108163.
- Griffith, O.L., Liu, X., Amonoo, J.A., Djurovich, P.I., Thompson, M.E., Green, P.F., and Forrest, S.R. (2015). Charge transport and exciton dissociation in organic solar cells consisting of dipolar donors mixed with C70. *Phys. Rev. B* 92, 085404.
- Liu, X., Li, Y., Ding, K., and Forrest, S. (2019). Energy loss in organic photovoltaics: Nonfullerene versus fullerene acceptors. *Phys. Rev. Appl.* 11, 024060.
- Li, D., Sun, C., Yan, T., Yuan, J., and Zou, Y. (2021). Asymmetric Non-Fullerene Small-Molecule Acceptors toward High-Performance Organic Solar Cells. *ACS Cent. Sci.* 7, 1787–1797.
- Che, X., Li, Y., Qu, Y., and Forrest, S.R. (2018). High fabrication yield organic tandem photovoltaics combining vacuum- and solution-processed subcells with 15% efficiency. *Nat. Energy* 3, 422–427.
- Che, X., Chung, C.-L., Hsu, C.-C., Liu, F., Wong, K.-T., and Forrest, S.R. (2018). Donor–Acceptor–Acceptor's Molecules for Vacuum-Deposited Organic Photovoltaics with Efficiency Exceeding 9%. *Adv. Energy Mater.* 8, 1703603.

8. Liu, F., Gu, Y., Wang, C., Zhao, W., Chen, D., Brisenio, A.L., and Russell, T.P. (2012). Efficient Polymer Solar Cells Based on a Low Bandgap Semi-crystalline DPP Polymer-PCBM Blends. *Adv. Mater.* **24**, 3947–3951.
9. Lin, L.-Y., Chen, Y.-H., Huang, Z.-Y., Lin, H.-W., Chou, S.-H., Lin, F., Chen, C.-W., Liu, Y.-H., and Wong, K.-T. (2011). A Low-Energy-Gap Organic Dye for High-Performance Small-Molecule Organic Solar Cells. *J. Am. Chem. Soc.* **133**, 15822–15825.
10. Zhang, T., Han, H., Zou, Y., Lee, Y.C., Oshima, H., Wong, K.T., and Holmes, R.J. (2017). Impact of Thermal Annealing on Organic Photovoltaic Cells Using Regioisomeric Donor-Acceptor-Acceptor Molecules. *ACS Appl. Mater. Interfaces* **9**, 25418–25425.
11. Zhan, L., Li, S., Li, Y., Sun, R., Min, J., Bi, Z., Ma, W., Chen, Z., Zhou, G., Zhu, H., et al. (2022). Desired open-circuit voltage increase enables efficiencies approaching 19% in symmetric-asymmetric molecule ternary organic photovoltaics. *Joule* **6**, 662–675.
12. He, C., Bi, Z., Chen, Z., Guo, J., Xia, X., Lu, X., Min, J., Zhu, H., Ma, W., Zuo, L., and Chen, H. (2022). Compromising Charge Generation and Recombination with Asymmetric Molecule for High-Performance Binary Organic Photovoltaics with Over 18% Certified Efficiency. *Adv. Funct. Mater.* **32**, 2112511.
13. Tang, C., Ma, X., Wang, J.Y., Zhang, X., Liao, R., Ma, Y., Wang, P., Wang, P., Wang, T., Zhang, F., and Zheng, Q. (2021). High-Performance Ladder-Type Heteroheptacene-Based Nonfullerene Acceptors Enabled by Asymmetric Cores with Enhanced Noncovalent Intramolecular Interactions. *Angew. Chem., Int. Ed. Engl.* **60**, 19314–19323.
14. He, C., Chen, Z., Wang, T., Shen, Z., Li, Y., Zhou, J., Yu, J., Fang, H., Li, Y., Li, S., et al. (2022). Asymmetric electron acceptor enables highly luminescent organic solar cells with certified efficiency over 18%. *Nat. Commun.* **13**, 2598–2611.
15. Wang, J., Chen, H., Xu, X., Ma, Z., Zhang, Z., Li, C., Yang, Y., Wang, J., Zhao, Y., Zhang, M., et al. (2022). An acceptor with an asymmetric and extended conjugated backbone for high-efficiency organic solar cells with low nonradiative energy loss. *J. Mater. Chem. A* **10**, 16714–16721.
16. Li, Y., Huang, X., Mencke, A.R., Kandappa, S.K., Wang, T., Ding, K., Jiang, Z.-Q., Amassian, A., Liao, L.S., Thompson, M.E., and Forrest, S.R. (2023). Interactions between non-fullerene acceptors lead to unstable ternary organic photovoltaic cells. *Proc. Natl. Acad. Sci. USA* **120**, e2301118120.
17. Burlingame, Q., Ball, M., and Loo, Y.L. (2020). It's time to focus on organic solar cell stability. *Nat. Energy* **5**, 947–949.
18. Bhattacharya, P. (1997). *Semiconductor Optoelectronic Devices* (Prentice Hall).
19. Ding, K., Huang, X., Li, Y., and Forrest, S.R. (2021). Photogeneration and the bulk quantum efficiency of organic photovoltaics. *Energy Environ. Sci.* **14**, 1584–1593.
20. Kirkpatrick, S., Gelatt, C.D., and Vecchi, M.P. (1983). Optimization by Simulated Annealing. *Science* **220**, 671–680.
21. Neumann, T., Danilov, D., Lennartz, C., and Wenzel, W. (2013). Modeling disordered morphologies in organic semiconductors. *J. Comput. Chem.* **34**, 2716–2725.
22. Friederich, P., Coehoorn, R., and Wenzel, W. (2017). Molecular Origin of the Anisotropic Dye Orientation in Emissive Layers of Organic Light Emitting Diodes. *Chem. Mater.* **29**, 9528–9535.
23. Coehoorn, R., Lin, X., Weijtens, C.H.L., Gottardi, S., and Van Eersel, H. (2021). Three-Dimensional Modeling of Organic Light-Emitting Diodes Containing Molecules with Large Electric Dipole Moments. *Phys. Rev. Appl.* **16**, 034048.
24. Groves, C., and Greenham, N.C. (2014). Monte Carlo Simulations of Organic Photovoltaics. *Top. Curr. Chem.* **352**, 257–278.
25. Metropolis, N., Rosenbluth, A.W., Rosenbluth, M.N., Teller, A.H., and Teller, E. (2004). Equation of State Calculations by Fast Computing Machines. *J. Chem. Phys.* **21**, 1087–1092.
26. Haillant, O., Dumbleton, D., and Zielnik, A. (2011). An Arrhenius approach to estimating organic photovoltaic module weathering acceleration factors. *Sol. Energy Mater. Sol. Cells* **95**, 1889–1895.
27. Li, Y., Huang, X., Ding, K., Sheriff, H.K.M., Ye, L., Liu, H., Li, C.Z., Ade, H., and Forrest, S.R. (2021). Non-fullerene acceptor organic photovoltaics with intrinsic operational lifetimes over 30 years. *Nat. Commun.* **12**, 5419–9.
28. Burlingame, Q., Huang, X., Liu, X., Jeong, C., Coburn, C., and Forrest, S.R. (2019). Intrinsically stable organic solar cells under high-intensity illumination. *Nature* **573**, 394–397.
29. Afolayan, E.O., Dursun, I., Lang, C., Pakhomenko, E., Kondakova, M., Boroson, M., Hickner, M., Holmes, R.J., and Giebink, N.C. (2022). Reducing Spontaneous Orientational Polarization via Semiconductor Dilution Improves OLED Efficiency and Lifetime. *Phys. Rev. Appl.* **17**, L051002.
30. He, S., Pakhomenko, E., and Holmes, R.J. (2023). Process Engineered Spontaneous Orientation Polarization in Organic Light-Emitting Devices. *ACS Appl. Mater. Interfaces* **15**, 1652–1660.
31. Pakhomenko, E., and Holmes, R.J. (2022). The role of OLED emissive layer polarization in sub-turn-on charge accumulation. *Proc. SPIE 12208. Org. Hybrid Light Emit. Mater. Devices XXVI 122080A*.
32. Esaki, Y., Tanaka, M., Matsushima, T., and Adachi, C. (2021). Active Control of Spontaneous Orientation Polarization of Tris(8-hydroxyquinolinato)aluminum (Alq3) Films and Its Effect on Performance of Organic Light-Emitting Diodes. *Adv. Electron. Mater.* **7**, 2100486.
33. Noguchi, Y., Brütting, W., and Ishii, H. (2019). Spontaneous orientation polarization in organic light-emitting diodes. *Jpn. J. Appl. Phys.* **58**, SF0801.
34. Noguchi, Y., Miyazaki, Y., Tanaka, Y., Sato, N., Nakayama, Y., Schmidt, T.D., Brütting, W., and Ishii, H. (2012). Charge accumulation at organic semiconductor interfaces due to a permanent dipole moment and its orientational order in bilayer devices. *J. Appl. Phys.* **111**, 114508.
35. Pakhomenko, E., He, S., and Holmes, R.J. (2022). Polarization-Induced Exciton-Polaron Quenching in Organic Light-Emitting Devices and Its Control by Dipolar Doping. *Adv. Opt. Mater.* **10**, 2201348.
36. Baldo, M.A., and Forrest, S.R. (2001). Interface-limited injection in amorphous organic semiconductors. *Phys. Rev. B* **64**, 085201.
37. Schmidt, T.D., Jäger, L., Noguchi, Y., Ishii, H., and Brütting, W. (2015). Analyzing degradation effects of organic light-emitting diodes via transient optical and electrical measurements. *J. Appl. Phys.* **117**, 215502.
38. Scholz, S., Kondakov, D., Lüssem, B., and Leo, K. (2015). Degradation mechanisms and reactions in organic light-emitting devices. *Chem. Rev.* **115**, 8449–8503.
39. Yamada, T., Zou, D., Jeong, H., Akaki, Y., and Tsutsui, T. (2000). Recoverable degradation and internal field forming process accompanied by the orientation of dipoles in organic light emitting diodes. *Synth. Met.* **111–112**, 237–240.